PNAS RESEARCH ARTICLE | BIOCHEMISTRY

Molecular basis of hemoglobin binding and heme removal in *Corynebacterium diphtheriae*

Brendan J. Mahoney[a,b], Lindsey R. Lyman[c], Jordan Ford[a], Jess Soule[a], Nicole A. Cheung[b,d], Andrew K. Goring[a], Kat Ellis-Guardiola[a,b], Michael J. Collazo[b], Duilio Cascio[b], Hung Ton-That[d,e], Michael P. Schmitt[c,1], and Robert T. Clubb[a,b,d,1]

Edited by Arthur Palmer, Columbia University, New York, NY; received June 12, 2024; accepted December 6, 2024

To successfully mount infections, nearly all bacterial pathogens must acquire iron, a key metal cofactor that primarily resides within human hemoglobin. *Corynebacterium diphtheriae* causes the life-threatening respiratory disease diphtheria and captures hemoglobin for iron scavenging using the surface-displayed receptor HbpA. Here, we show using X-ray crystallography, NMR, and in situ binding measurements that *C. diphtheriae* selectively captures iron-loaded hemoglobin by partially ensconcing the heme molecules of its α subunits. Quantitative growth and heme release measurements are compatible with *C. diphtheriae* acquiring heme passively released from hemoglobin's β subunits. We propose a model in which HbpA and heme-binding receptors collectively function on the *C. diphtheriae* surface to capture hemoglobin and its spontaneously released heme. Acquisition mechanisms that exploit the propensity of hemoglobin's β subunit to release heme likely represent a common strategy used by bacterial pathogens to obtain iron during infections.

hemoglobin | NMR | X-ray crystallography | bacterial growth | heme capture

Significance

During infections, microbial pathogens scavenge heme-iron from human hemoglobin released from lysed red blood cells. We have learned how *Corynebacterium diphtheriae* uses its HbpA receptor to capture hemoglobin on its cell surface. A process in which this pathogen acquires spontaneously released heme from hemoglobin provides sufficient iron to sustain bacterial growth. We propose that this is a common strategy used by microbial pathogens to scavenge heme-iron from hemoglobin.

Corynebacterium diphtheriae is the causative agent of the severe upper respiratory disease diphtheria. Since its discovery by Edwin Klebs and Friedrich Löffler, studies of this pathogen have greatly impacted our understanding of how changes in extracellular iron levels impact microbial growth and virulence (1–3). Upon encountering an iron-deplete environment within its human host, transcriptional changes triggered by the microbial DtxR repressor produce the diphtheria toxin that causes paralysis and congestive heart failure, as well as hemophores and small molecule siderophores that scavenge iron (2, 4–7). Human hemoglobin (Hb) within red blood cells contains ~75 to 80% of the body's iron content in the form of heme (iron-protoporphyrin IX) and is actively targeted by *C. diphtheriae* as a nutrient source (8–15). When red blood cells are lysed Hb is released into the surrounding plasma where its heme molecules are rapidly oxidized to their ferric state (called hemin). This form of Hb is referred to as methemoglobin (metHb) and it has a greater propensity to dissociate into αβ heterodimers upon Hb dilution outside of cells (16, 17). Dimeric metHb has weaker affinity for hemin, with the αHb subunit binding hemin with higher affinity than βHb. Further dissociation of dimeric metHb into its component hemin-bound globins can also occur, with the isolated globins exhibiting the weakest affinity for hemin. To limit infections, humans have developed innate nutritional immunity mechanisms that limit the amount of available iron. In particular, free iron or hemin is bound by the plasma proteins transferrin and hemopexin, respectively, or they are both bound by human serum albumin (18, 19). In addition, iron-laden metHb released from lysed red blood cells is bound by the abundant human plasma protein haptoglobin (Hp) and subsequently removed from the blood by macrophages via CD163-mediated endocytosis (20–22). During infections, *C. diphtheriae* and other bacterial pathogens circumvent this process by acquiring hemin from metHb and the metHb–Hp complex, and in some instances by blocking metHb–Hp removal from the blood (13, 23–26). Hemin-uptake systems in several species of gram-positive bacteria within the Bacillota phylum (formerly known as Firmicutes) have been characterized that employ structurally related NEAr-iron Transporter (NEAT) domains to capture hemin and metHb (27, 28). In contrast, despite its discovery over a century ago, much less is known about the molecular basis of hemin uptake from metHb by pathogenic *C. diphtheriae* and related species of Actinomycetota (formerly known as Actinobacteria) which use structurally distinct protein machinery to harvest hemin.

The hemin-uptake system in *C. diphtheriae* is composed of at least 10 proteins that collectively capture hemin from host hemoproteins and import it into the cytoplasm where it is degraded to release free iron (Fig. 1). The core machinery found in most strains is encoded by genes expressed from the *hmu* hemin import locus, which produces a membrane-embedded HmuTUV ABC transporter that imports hemin across the plasma

Author affiliations: [a]Department of Chemistry and Biochemistry, University of California, Los Angeles, CA 90095; [b]University of California, Los Angeles-United States Department of Energy Institute of Genomics and Proteomics, University of California, Los Angeles, CA 90095; [c]Laboratory of Respiratory and Special Pathogens, Division of Bacterial, Parasitic, and Allergenic Products, Center for Biologics Evaluation and Research, Food and Drug Administration, Silver Spring, MD 20903; [d]Molecular Biology Institute, University of California, Los Angeles, CA 90095; and [e]Division of Oral and Systemic Health Sciences, School of Dentistry, University of California, Los Angeles, CA 90095

Author contributions: B.J.M., L.R.L., K.E.-G., H.T.-T., M.P.S., and R.T.C. designed research; B.J.M., L.R.L., J.F., J.S., N.A.C., K.E.-G., and M.J.C. performed research; J.F. and A.K.G. contributed new reagents/analytic tools; B.J.M., L.R.L., J.F., J.S., N.A.C., A.K.G., and D.C. analyzed data; and B.J.M., L.R.L., H.T.-T., M.P.S., and R.T.C. wrote the paper.

The authors declare no competing interest.

This article is a PNAS Direct Submission.

[1]To whom correspondence may be addressed. Email: michael.schmitt@fda.hhs.gov or rclubb@mbi.ucla.edu.

This article contains supporting information online at https://www.pnas.org/lookup/suppl/doi:10.1073/pnas.2411833122/-/DCSupplemental.

Published December 31, 2024.

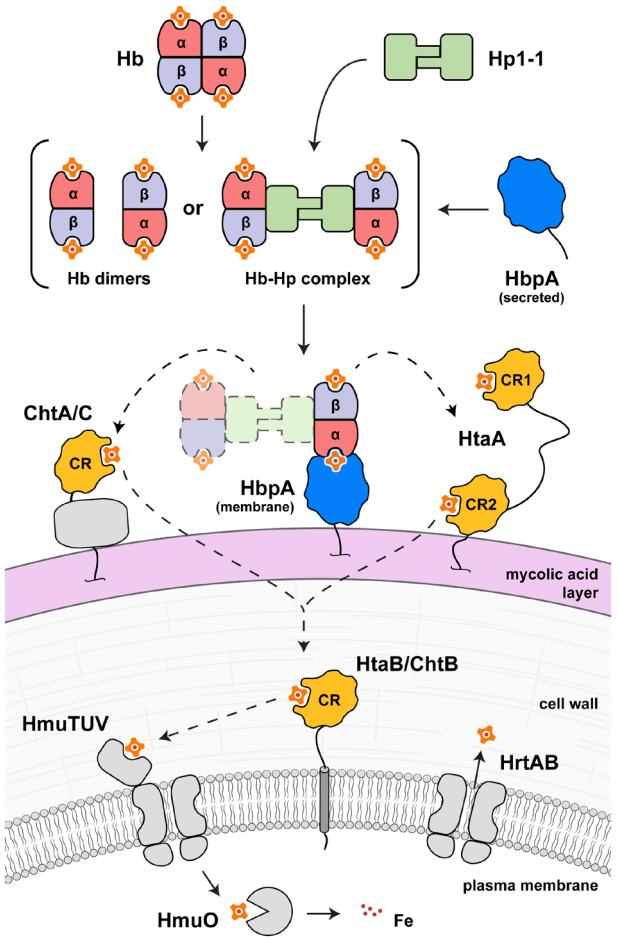

Fig. 1. Schematic of *C. diphtheriae* hemin acquisition pathway. Upon release from red blood cells, tetrameric Hb rapidly dissociates into metHb dimers. Hemin passively released from the β subunit of metHb (or metHb–Hp) bound to HbpA is captured by surface-exposed CR domain-containing receptors ChtA, ChtC, or HtaA. Hemin is then relayed to the HmuTUV integral membrane ABC transporter, presumably involving transfer via HtaB or ChtB, and degraded by the heme oxygenase HmuO. Excess hemin is exported by the HrtAB efflux pump. Only the Hp1-1 form of Hp is shown. Also shown in the figure are secreted forms of the HbpA receptor that bind metHb and the metHb–Hp complex.

membrane into the cytoplasm (29, 30). This gene locus also encodes for the surface-displayed HtaA and HtaB hemin-binding receptors, which are embedded into the membrane via C-terminal transmembrane (TM) helices (4, 29, 31). HtaA and HtaB bind hemin via conserved region (CR) domains that have recently been shown to coordinate its central iron atom via a conserved tyrosine residue (32–35). The core hemin-uptake system is completed by HmuO, an oxygenase that degrades hemin to release free iron after it has been imported into the cytoplasm by the HmuTUV complex (36–38). Epidemic strains responsible for a lethal 1990s outbreak of diphtheria in the former Soviet Union supplement the core machinery with additional hemin- and Hb-binding proteins (39, 40). These include three surface proteins that bind hemin via CR domains (ChtA, ChtB, and ChtC) and HbpA, which binds to metHb and the metHb–Hp complex (24, 25, 40). Based on the positioning and activities of these proteins, HbpA may initiate the process of hemin capture by binding metHb on the cell surface. Released hemin is then passed across the cell wall via the CR domain-containing receptors, imported by the HmuTUV complex, and then degraded by HmuO to release iron. Because hemin is toxic when it is present at elevated concentrations, *C. diphtheriae* maintains homeostasis using the membrane-embedded HrtAB complex which exports hemin from the cytoplasm when it becomes too abundant (41, 42). Studies of *C. diphtheriae* gene deletion mutants have revealed that microbial growth on hemin is reliant on HmuTUV, HtaA, and either HtaB or ChtB, while growth on the metHb–Hp complex also requires the expression of HbpA and either ChtA or ChtC (24, 25).

Here, we report the results of cellular, structural, biochemical, and growth modeling experiments that provide insight into how *C. diphtheriae* uses its HbpA receptor to scavenge hemin from human metHb. A crystal structure of the HbpA–Hb complex and NMR studies reveal that the receptor captures only the heme-loaded form of Hb by contacting heme molecules bound to its α subunit. Bacteria harboring receptor mutations located within the HbpA–Hb interface are impaired both in their ability to bind to metHb and to use the metHb–Hp complex as a nutrient. Surprisingly, despite sharing only limited primary sequence homology, HbpA and CR domains within *C. diphtheriae*'s hemin-uptake system are structurally related. Based on the structure and quantitative rate measurements of Hb-dependent growth, we propose that *C. diphtheriae* passively acquires hemin from hemoglobin and present a model for how this process occurs on the cell surface.

Results

The HbpA Receptor Binds to Human Hb Using a CR-Like Domain. We have previously shown that HbpA residues 32 to 322 ($HbpA^S$) form a water-soluble ectodomain that binds to Hb (25). To delineate the minimal region within $HbpA^S$ that binds to Hb, a series of truncation constructs were tested using NMR spectroscopy (*SI Appendix*, Fig. S1 *A* and *B*). This analysis revealed that residues 33 to 229 ($HbpA^{\Delta 229}$) adopt a folded structure that is sufficient to bind Hb (Fig. 2*A* and *SI Appendix*, Fig. S1 *C* and *D*). Using standard multidimensional heteronuclear NMR methods, we determined the solution structure of $HbpA^{\Delta 229}$; an ensemble of 20 conformers represents the structure of $HbpA^{\Delta 229}$ and is in good agreement with the experimental data (Fig. 2*B* and *SI Appendix*, Fig. S2 and Table S1). The structure of the protein is well defined by the NMR data, with the exception of two partially disordered surface loops that connect strands β4 to β5 (E107-H110) and β6 to β7 (G126-D129), which experience local dynamics as assessed by backbone relaxation experiments (*SI Appendix*, Fig. S3). $HbpA^{\Delta 229}$ adopts an elongated structure that is constructed from two subdomains (Fig. 2*C*). The "terminal" subdomain contains the N and C termini of the protein and adopts a β-sandwich structure formed from two antiparallel β-sheets (strands β4b, β5, β7b, β8, β9a, and strands β3, β4a, β1, β11, β10, β9b, respectively) (Fig. 2*C*, green). The adjacently positioned "distal" subdomain adopts a splayed α/β structure that contains four α-helices (α1-α4, Fig. 2*C*, cyan) and several surface loops that pack against a third, smaller β-sheet (β2, β6, β7a, β8, Fig. 2*C*, slate). Two extended loops that connect the β10-α2 and α3-α4 structural elements in the distal subdomain are linked by a disulfide bond (between C182 and C211) which is likely important for protein stability as its reduction causes protein precipitation (Fig. 2*C*, yellow sticks). Surprisingly, although they share only ~14 to 18% primary sequence identity, the structures of $HbpA^{\Delta 229}$ and hemin-binding CR domains are related (32, 33). In particular, both types of proteins possess related β-sandwich terminal subdomains (Fig. 3, green); the backbone atoms of residues forming strands β4b-β5-β7b-β8 and β1-β11-β10-β9b (colored green) in HbpA and CR domains can be superimposed with a coordinate RMSD of ~2.5 to 2.7 Å. However, the structures of their distal subdomains, which in CR domains are the site of hemin binding, differ substantially (Fig. 3*B*, red box). As compared to CR domains,

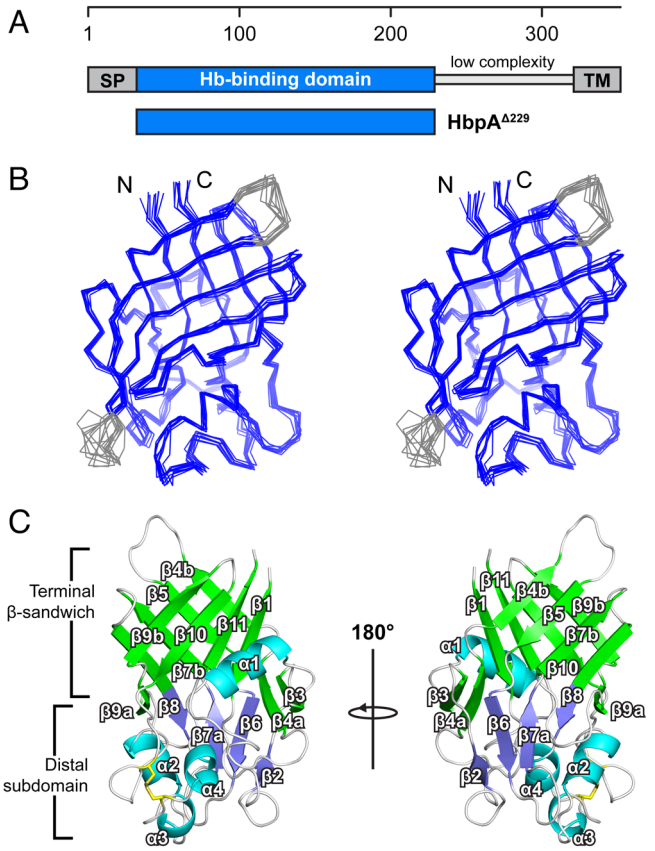

Fig. 2. NMR structure of HbpA. (*A*) Domain schematic of the HbpA Hb receptor, with its signal peptide (SP) and single TM helix indicated. A region of low amino acid sequence complexity connects the TM helix to the structured domain that binds to Hb (residues 33 to 229, HbpA$^{\Delta 229}$). (*B*) Stereo view showing the ensemble of 10 lowest energy NMR structures of HbpA$^{\Delta 229}$. The N and C termini are indicated, and the partially disordered β5-β6 and β6-β7 loops are colored gray. (*C*) Cartoon depiction of HbpA$^{\Delta 229}$, with two views shown that are related by a 180° rotation. Secondary structure elements are labeled with α-helices colored cyan. Residues forming the β-sandwich in the terminal subdomain are colored green and residues forming the β-sheet in the distal subdomain are colored slate. The disulfide bond (C182-C211) is shown as stick representation in yellow.

the distal subdomain in HbpA contains a different ordering of its secondary structural elements between strands β1 and β4 (elements β2-β3-α1 in HbpA vs. α1-β2-β3 in CR domains), as well as a large multihelix insertion between strands β10 and β11 that is absent in CR domains [HbpA contains three contiguous helices (α2-α4) instead of the single helix]. These differences may explain why HbpA is incapable of binding hemin. Most notably, in CR domains hemin binding is mediated by a conserved iron-coordinating tyrosine residue that is located within its α1 helix (32–35), whereas in HbpA the helix is replaced with two short helical turns and an intervening β1-β2 loop. Moreover, the cleft in CR domains that is used to ensconce the hemin is missing in HbpA because it is filled by residues located in helices α3 and α4. Intriguingly, several HbpA residues in this region exhibit elevated mobility, which is commonly observed in unliganded binding surfaces (*SI Appendix*, Fig. S3).

Crystal Structure of the HbpA–Hb Complex. To gain insight into the molecular basis of Hb binding, we determined the 1.69 Å crystal structure of the HbpA$^{\Delta 229}$–Hb complex. Complete data collection and structural statistics are present in *SI Appendix*, Table S2. In the structure two HbpA$^{\Delta 229}$ molecules bind to a metHb tetramer (Fig. 4*A*); in the crystal this complex is constructed from two asymmetric units that each contain a single chain of HbpA$^{\Delta 229}$ bound to a αβ heterodimer. This binding stoichiometry is consistent with solution multiangle light scattering experiments, which indicate that only two HbpA$^{\Delta 229}$ proteins engage a single Hb tetramer even when the receptor is present at fourfold molar excess (*SI Appendix*, Fig. S4). The structure sheds light onto how the receptor engages physiologically relevant dimeric forms of metHb that are either free in solution or bound to Hp, since the metHb surface contacted by the receptor in the HbpA$^{\Delta 229}$–Hb complex remains exposed in these forms of metHb.

In the structure of the HbpA$^{\Delta 229}$–Hb complex, the hemin-binding pocket within each of metHb's α subunits (αHb) is bound by a single HbpA protein via residues located in the receptor's β1-β2 and β6-β7 loops, as well as its α3-α4 helices. Within the β1-β2 loop, HbpA residue Y52 engages in electrostatic interactions with αHb's EF loop, while the side chain of N55 interacts with the backbone carbonyl and amide groups of residues N78 and A82 within the F-helix, respectively (Fig. 4*B*). Adjacent to this contact surface, Y127's aromatic sidechain within the β6-β7 loop packs into a gap that is located between Hb's E and F helices, while hemin's exposed D-ring propionate group is positioned to form direct and water-mediated hydrogen bonding interactions with the backbone atoms of L125 and G126, as well as the side chain of K202 (Fig. 4*C*). The interface is completed by contacts between αHb's F-helix and residues within the α3 and α4 helices in HbpA (Fig. 4*D*). HbpA α3 residues L201 and V204 form van der Waals packing interactions with αHb's F-helix, while D215 and K218 in the α4 helix are positioned to form salt bridge interactions with the side chains of αHb residues R141 and D85, respectively. Interestingly, this region in the receptor also contacts the CD loop in the neighboring βHb globin chain (*SI Appendix*, Fig. S5*A*). However, interactions between HbpA and αHb's hemin pocket are likely the primary determinant for binding affinity as the HbpA–αHb interface constitutes 77% of the total buried surface area in the complex (each HbpA protein buries a total of 1,091 Å^2 when it binds to the Hb tetramer) (43, 44). HbpA's preference for αHb may originate from receptor contacts to its F-helix, as this surface is distinct in the two types of globins. In αHb the F-helix contains A79 and A82 side chains that are contacted by HbpA, while in βHb these residues are replaced with larger threonine side chains that presumably form weaker interactions with the receptor (T84 and T87). Preferential binding over αHb's hemin pocket may also be provided by supplemental and potentially stabilizing contacts to the neighboring βHb in the Hb tetramer. The converse is not true, since manually built models of the complex in which HbpA is instead positioned over βHb's pocket within the Hb tetramer do not result in additional receptor contacts to the adjacent αHb chain (*SI Appendix*, Fig. S5*B*). Receptor binding causes only minor changes in the structure of Hb as its heavy atom backbone coordinates can be superimposed with the structures of the isolated carbonmonoxy form of Hb (HbCO) (PDB: 6KAV) and metHb (PDB: 6NBC) with RMSD values of 0.67 and 0.51 Å, respectively (45, 46). However, subtle changes in the structure and dynamics of the receptor do accompany binding, including conformational ordering of the aforementioned dynamic β6-β7 loop and repositioning of residues within the adjacent α3 helix.

HbpA Selectively Binds to Holo-Hb without Blocking Heme Release from Its β Subunit. In the crystal structure, interactions between the receptor and αHb's hemin suggest that HbpA may selectively recognize only the heme-loaded form of Hb. To investigate this issue, NMR was used to monitor [U-^{15}N] HbpA$^{\Delta 229}$ binding to either heme-loaded or -free forms of Hb. Consistent with the structure of the complex, when heme-loaded HbCO is added to a sample of [U-^{15}N] HbpA$^{\Delta 229}$ its ^{1}H-^{15}N

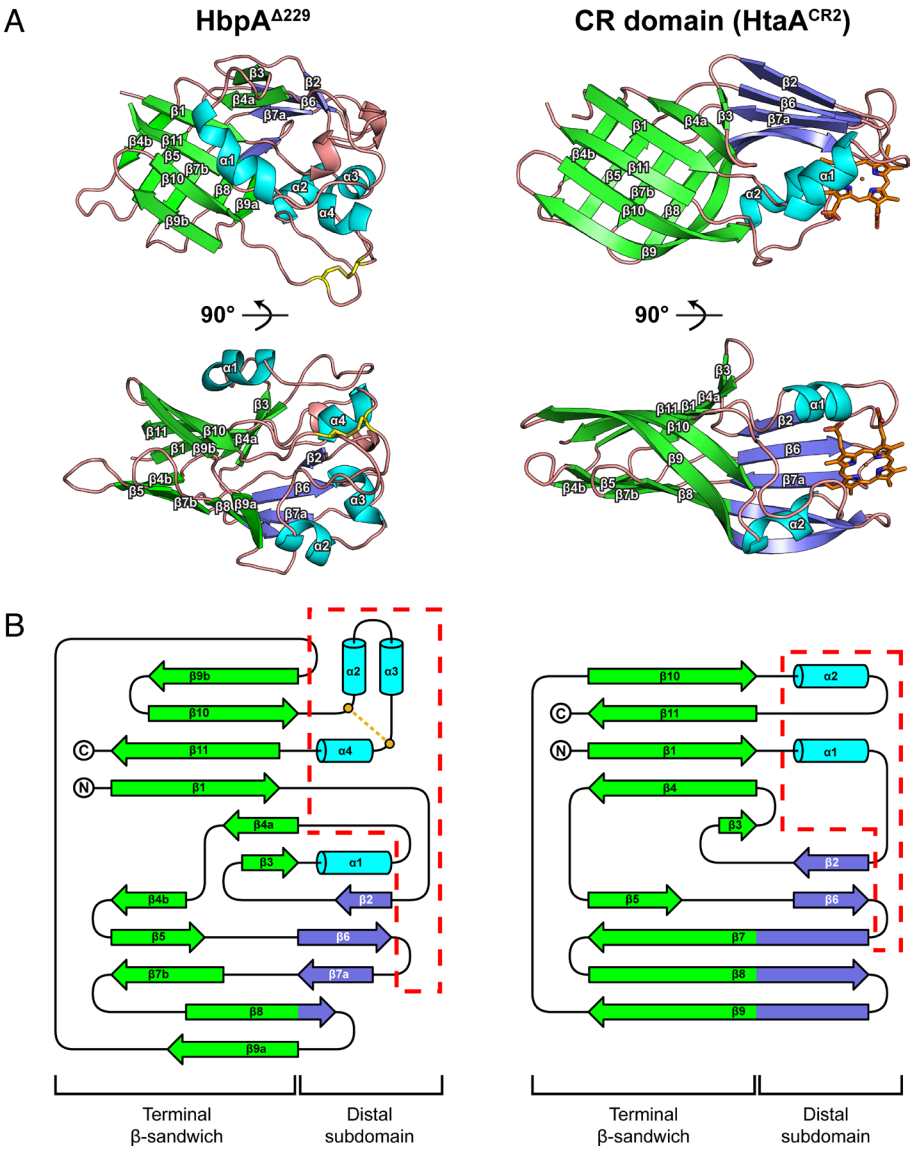

Fig. 3. HbpA and CR domains within the hemin-uptake system are structurally related. (*A*) Two views of HbpA$^{\Delta 229}$ related by a 90° rotation (*Left*) and similar views of the hemin-binding C-terminal CR domain from the *C. diphtheriae* HtaA protein (HtaA^{CR2}, PDB: 8SMU) (*Right*) (33). The largest structural differences occur in regions responsible for hemin binding in CR domains. (*B*) Secondary structure topology diagrams of HbpA$^{\Delta 229}$ (*Left*) and HtaA^{CR2} (*Right*). The proteins are constructed from "terminal" and "distal" subdomains. Color code: the β-strands in the terminal subdomain (green), strands in the β-sheet within the distal subdomain (slate), α-helices (cyan), and disulfide bond (gold). Regions in HtaA^{CR2} involved in hemin binding are enclosed within a dashed red box. The analogous region in HbpA$^{\Delta 229}$ mediates binding to metHb in the crystal structure of the complex described later (dashed red box).

HSQC spectrum exhibits substantial line broadening indicative of the formation of a high molecular weight Hb–receptor complex (Fig. 5*A*). Conversely, only limited spectral changes are observed when Hb lacking heme (apo-Hb) is added at fourfold molar excess (Fig. 5*B*), suggesting that contacts to αHb's hemin are important for receptor binding. However, it is also possible that hemin loss from Hb causes changes in the conformation and/or dynamics of the surrounding globin residues that impair receptor binding, since in apo-Hb the hemin binding pocket has been shown to exchange between folded and molten states (47). Interestingly, similar NMR experiments reveal that HbpA$^{\Delta 229}$ does not bind with appreciable affinity to heme-loaded myoglobin (Mb), a structurally related member of the globin family (*SI Appendix*, Fig. S6*A*). Thus, our results indicate that HbpA preferentially binds to Hb only when it carries heme and not empty Hb dimers, which presumably maximizes the ability of *C. diphtheriae* to exploit this abundant source of iron as a nutrient.

To ascertain whether receptor binding promotes hemin release from Hb we employed H64Y/V68F apo-myoglobin (apo-Mb$^{H64Y/V68F}$), an established hemin scavenging reagent with unique spectral properties (17, 48, 49). As expected, upon mixing metHb with an excess of apo-Mb$^{H64Y/V68F}$ biphasic time-dependent UV-Vis spectral changes are observed at 405 nm (A_{405}) that report on the rate of spontaneous hemin release from Hb into the solvent and its subsequent capture by apo-Mb$^{H64Y/V68F}$ (Fig. 5*C*, black curve). The rapid and slow spectral changes are defined by k_{fast} and k_{slow} rate constants that report on hemin loss from the βHb and αHb chains, respectively. Interestingly, adding increasing amounts of HbpA$^{\Delta 229}$ (0 to 250 μM) to this reaction mixture progressively eliminates the slower spectral changes attributed to hemin loss from αHb, while leaving the rapid changes associated with hemin release from βHb unperturbed (adding up to ~50-fold HbpA$^{\Delta 229}$ decreases k_{fast} by only ~2.5-fold, but completely eliminates the slower spectral changes) (Fig. 5*C* and *SI Appendix*, Table S3). Tracking the total hemin lost from metHb as a function of added

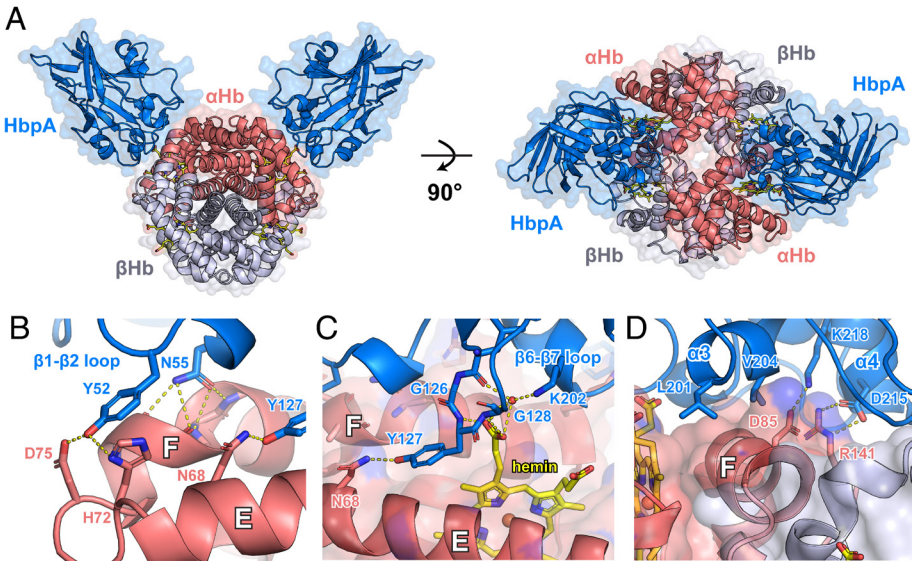

Fig. 4. Structure of the HbpA complex with hemoglobin. (*A*) Crystal structure of HbpA bound to human Hb reveals two receptors bind to the metHb tetramer, each partially capping the hemin molecule located within the tetramer's α subunits. (*B*) Magnified view of interactions between HbpA β1 and β2 loop and the EF region of αHb at the edge of the protein–protein interface. The E and F helices of αHb are indicated. (*C*) View of interactions between HbpA's β6 and β7 loop and a hemin propionate group at the HbpA–αHb interface. (*D*) Residues in HbpA's α3 and α4 helices bind over the αHb F-helix via a combination of van der Waals packing and salt bridge interactions.

HbpA$^{\Delta 229}$ reveals that when the receptor is present in excess, only ~50% of Hb's hemin is released after 20 h (Fig. 5*D*). These findings suggest that HbpA$^{\Delta 229}$ blocks hemin release from αHb without perturbing hemin egress from the βHb subunit.

Disrupting Hb Binding by HbpA Impairs *C. diphtheriae*'s Ability to Use the Hb–Hp Complex as an Iron Source. We determined how the receptor–Hb interactions visualized in the crystal structure affected *C. diphtheriae*'s ability to capture Hb and use it as a nutrient source. *C. diphtheriae* strain 1737 deleted for the *hbpA* gene (1737Δ*hbpA*) was transformed with a series of plasmids that expressed either full-length wild-type HbpA or protein variants containing single amino acid substitutions within the molecular interface (Y52A, N55A, Y127A, F206A, Fig. 4 *B*–*D*). Control experiments indicate that all of the mutant receptors are displayed on the bacterial surface similar to the wild-type HbpA (*SI Appendix*, Fig. S7*A*). Consistent with the crystal structure of the complex, whole-cell ELISA experiments indicate that cells displaying receptors with interfacial mutations are impaired in their ability to capture Hb (Fig. 6*A*, blue circles). These binding defects are comparable to the 1737Δ*hbpA* deletion strain, except for the N55A mutant that shows a more modest effect. The most severe binding defects are caused by substitutions that are predicted to disrupt receptor contacts to Hb's E and F helices that surround its hemin and by a previously reported F206A alteration that likely destabilizes the local structure of the receptor at the molecular interface (50). Whole-cell ELISA experiments also reveal that the Y52A, Y127A, and F206A substitutions disrupt binding to the Hb–Hp complex (Fig. 6*A*, red triangles). Interestingly, this finding is compatible with a model of the HbpA–Hb–Hp ternary complex built using our structure of the HbpA–Hb complex and a previously reported structure of the Hb–Hp complex (51). In the model of the complex, the receptor primarily contacts αHb's hemin pocket and does not sterically compete with Hp for Hb access (Fig. 6*E*). Binding experiments using an established in situ gel-based assay are in agreement with the whole-cell data, as they reveal that Y52A, Y127A, and F206A receptor variants are significantly impaired in their ability to bind to either Hb or the Hb–Hp complex (Fig. 6*B*). The whole-cell ELISA data further suggest that HbpA is the primary determinant for binding to either Hb or the Hb–Hp complex on the cell surface, as only small amounts of antibody-induced signal are observed in the Δ*hbpA* strain (Fig. 6*A*). This finding is consistent with fluorescence microscopy experiments comparing the WT and Δ*hbpA* deletion strains, since only the WT cells show significant Hb binding when probed using an anti-Hb antibody (Fig. 6*C*). Additionally, the prevalence of fluorescence signal on the periphery of these cells is in agreement with Hb binding to HbpA on the cell surface. Thus, our results are compatible with HbpA acting as the primary receptor for Hb and suggest that the interactions visualized in the structure of the HbpA$^{\Delta 229}$–Hb reveal how *C. diphtheriae* captures Hb and the Hb–Hp complex on the cell surface. *C. diphtheriae* 1737Δ*hbpA* cells lacking the HbpA receptor exhibit statistically significant, albeit small, defects in growth when they are cultured in media in which the Hb–Hp complex is the sole source of iron (25). This is apparent when the growth of 1737Δ*hbpA* cells complemented with an empty vector control is compared to 1737Δ*hbpA* cells that express the receptor (Fig. 6*D*, compare Δ*hbpA*/pKN to Δ*hbpA*/p-WT). Similar growth defects are observed for cells expressing Y127A and F206A receptor variants that are impaired in their ability to bind to Hb–Hp (and Hb) (Fig. 6*A*) (50). This suggests that tethering of the metHb–Hp complex to the microbial surface facilitates growth by enhancing the rate and/or efficiency of hemin removal. However, multiple factors other than iron removal from the metHb–Hp complex likely influence *C. diphtheriae* growth in cell culture, as cells displaying binding impaired Y52A and N55A variants are not growth impaired.

Secreted HbpA receptors have previously been shown to form extracellular aggregates that bind to Hb and the Hb–Hp complex (50, 52). All of the HbpA variants containing single amino acid substitutions in the Hb binding domain behave similar to the wild-type protein, as they are both displayed on the cell surface and capable of forming secreted aggregates (*SI Appendix*, Fig. S7). This is consistent with residues outside of the Hb-binding domain being responsible for aggregate formation and cell wall positioning. To further delineate protein regions important for cellular location, cells expressing receptors that lacked either the TM helix (HbpA^{S})

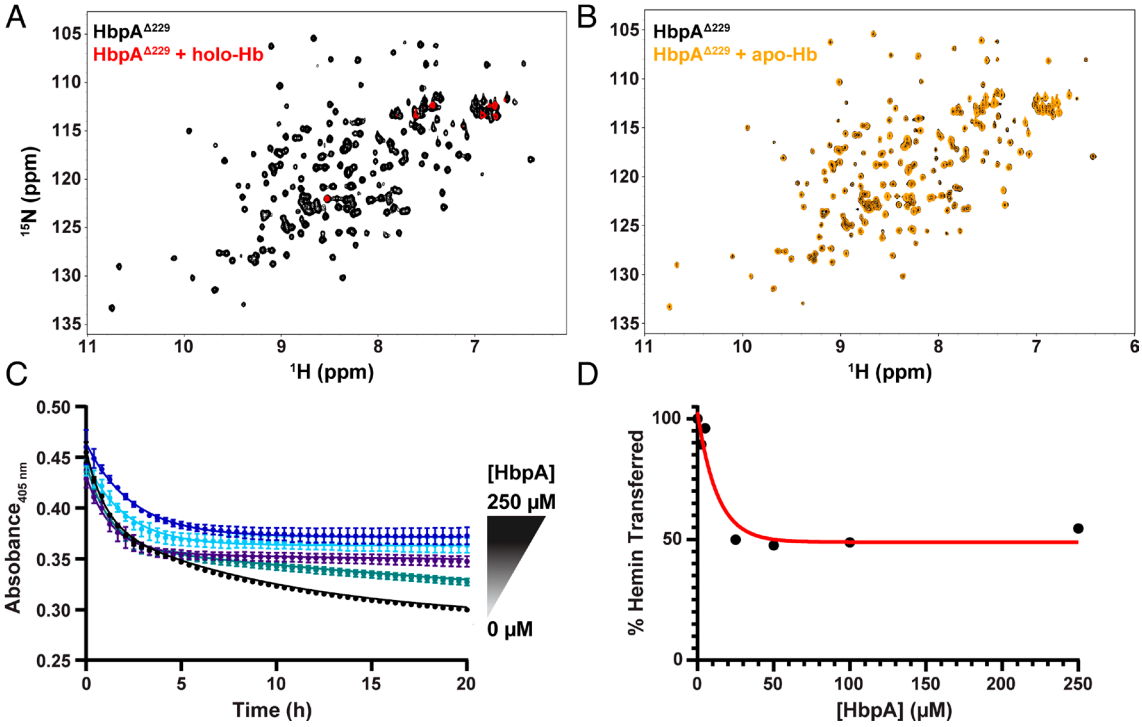

Fig. 5. HbpA binding to holo-Hb and its effects on in vitro hemin release. (*A*) Overlay of ^{1}H-^{15}N HSQC spectra of [U-^{15}N] HbpA$^{\Delta229}$ in the presence (red) or absence (black) of holo-Hb. The loss of signals upon adding holo-Hb is indicative of binding. In the experiment the carboxyhemoglobin (HbCO) form of Hb was used at a fourfold molar excess (200 μM, heme basis) relative to the receptor (50 μM). (*B*) As in panel (*A*) except the spectra show [U-^{15}N] HbpA$^{\Delta229}$ (50 μM) in either the presence (orange) or absence (black) of apo-Hb (200 μM, globin basis). The lack of significant spectral changes suggests that the receptor does not bind to apo-Hb with significant affinity. (*C*) Experiments monitoring hemin release from the ferric form of Hb (metHb) and subsequent capture by apo-Mb$^{H64Y/V68F}$. Spectral time courses show the change in the metHb Soret band absorbance (405 nm) after mixing with apo-Mb$^{H64Y/V68F}$. The amount of HbpA$^{\Delta229}$ was varied: 0 (black), 5 (green), 25 (purple), 100 (light blue), or 250 μM (dark blue) HbpA$^{\Delta229}$. Lines represent the exponential decay equation to which the data was fit, and error bars reflect the SD obtained from three replicates. Control experiments confirm that the absorbance changes are caused by hemin release from metHb and are not a result of HbpA$^{\Delta229}$ binding to either Hb or Mb (*SI Appendix*, Fig. S6 *B* and *C*). (*D*) Percent of hemin transferred as a function of HbpA$^{\Delta229}$ concentration. The % hemin transferred was determined by taking the ratio of ΔA_{405} at each HbpA$^{\Delta229}$ concentration to the ΔA_{405} in the absence of HbpA$^{\Delta229}$. Error bars representing the SE calculated by propagation of uncertainty are present but are too small to be observed at this scale. At saturating HbpA$^{\Delta229}$ concentrations, only 50% of the metHb-hemin molecules are released.

or the TM helix and residues that connect it to the Hb binding module (HbpA$^{\Delta229}$) were tested for their ability to either properly localize to the cell wall (*SI Appendix*, Fig. S7*A*), form extracellular aggregates (*SI Appendix*, Fig. S7*B*), bind to Hb and Hb–Hp complex (*SI Appendix*, Fig. S8), and use the Hb–Hp complex as an iron source (Fig. 6*D*). Compatible with the TM helix being the sole determinant for aggregation and proper cell wall localization, both HbpA^{S} and HbpA$^{\Delta229}$ fail to form aggregates and are impaired in their ability to bind the Hb–Hp complex on the cell surface and use it as a nutrient (Fig. 6*D* and *SI Appendix*, Fig. S8).

***C. diphtheriae* Growth Is Limited by the Rate of Passive Heme Release from Hb.** Based on our biochemical measurements that demonstrate receptor binding does not stimulate hemin release, we hypothesized that metHb captured on the cell surface by HbpA passively (spontaneously) releases its hemin. As such, the use of batch culture methods to monitor Hb-dependent growth would mask the receptor's importance. This is because any free hemin released from Hb in the batch culture, either tethered to WT cells via HbpA or free in solution when unable to bind to 1737Δ*hbpA* cells, could in principle rapidly diffuse and be captured by cells for import (53). To investigate this issue, we first determined the maximum growth rate (μ_{max}) at saturating Hb levels and the substrate saturation constant (K_s) for WT cells grown in varying concentrations of Hb to be 0.29 ± 0.01 h^{-1} and 0.56 ± 0.10 μM respectively (*SI Appendix*, Fig. S9). As WT and 1737Δ*hbpA* cells exhibit very similar growth behavior when Hb is the sole source of iron, we reasoned that K_s reports on the ability of the microbe to use hemin after it has been spontaneously released from Hb. Indeed, the growth data obtained for bacteria cultured in media containing varying amounts of Hb are accurately recapitulated using a modified Monod model and previously reported values for the rates of spontaneous hemin release from metHb (described in *SI Appendix* and illustrated in Fig. 7*A* and *SI Appendix*, Fig. S10) (17, 54, 55). In particular, there is a close correspondence between the experimentally derived and calculated specific growth rates for cells grown in a range of Hb concentrations (Fig. 7*B*), and as expected, the levels of unbound, "free" hemin, are very small (*SI Appendix*, Fig. S10*B*). This suggests that when cells are grown in batch culture the rate of spontaneous hemin release from Hb is growth limiting. Moreover, since WT and 1737Δ*hbpA* cells exhibit similar Hb-dependent growth kinetics, tethering Hb to the cell surface via HbpA does not accelerate the rate at which it loses its hemin. The growth model does not explicitly account for the effects of hemin degradation by HmuO or export by HrtAB, whose antagonistic effects on hemin usage have been previously modeled in *Corynebacterium glutamicum* (56). At very high metHb concentrations (>10 μM), impaired *C. diphtheriae* growth is observed that can no longer be adequately fit by our Monod model. This is presumably because the HmuO and HrtAB clearance systems fail to eliminate toxic levels of hemin. To avoid complications caused by these systems, we only modeled growth data obtained for cells cultured in lower, nontoxic levels of hemin. Under these conditions, our results show that spontaneous hemin

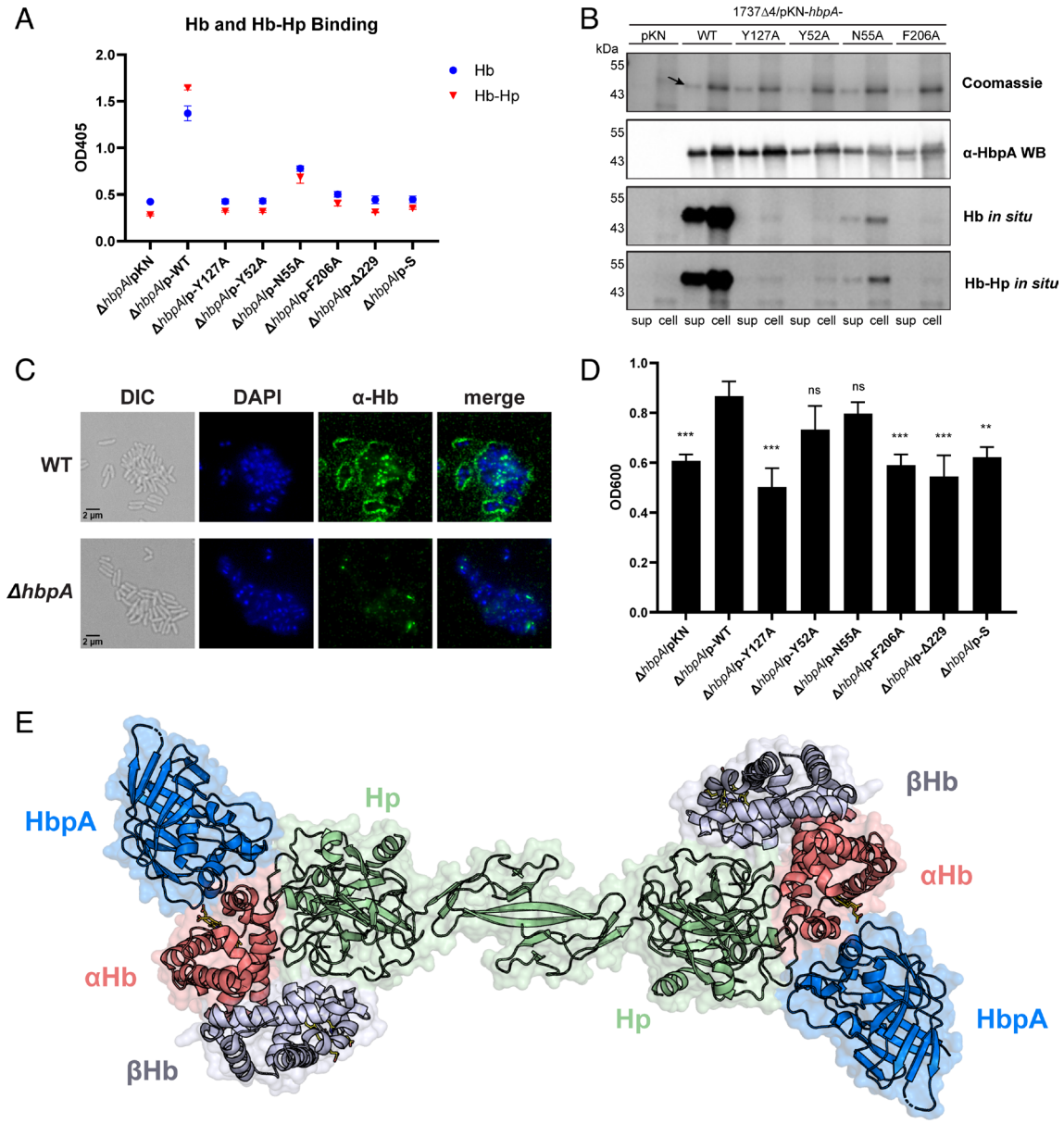

Fig. 6. Receptor mutations impair *C. diphtheriae*'s ability to capture the Hb–Hp complex. (*A*) Binding of *C. diphtheriae* cells to Hb (blue) and the Hb–Hp complex (red). Cell-based ELISA was used to detect protein binding to Δ*hbpA* cells expressing receptor variants from plasmid pKN2.6Z as previously described (52). pKN plasmids expressed: wild-type HbpA (Δ*hbpA*/p-WT), single amino acid variants (Δ*hbpA*/p-Y127A, Y52A, N55A, or F206A), only the Hb-binding domain (Δ*hbpA*/p-Δ229), or the full-length protein lacking its TM-helix (Δ*hbpA*/p-S). (*B*) Results of in situ gel binding of bacterial extracts to either Hb or the Hb–Hp complex. Cells were separated into supernatant fractions (sup, secreted proteins) and cell-associated proteins (cell). The strain used is *C. diphtheriae* 1737 that contains deletions of *hbpA*, *chtA*, *chtC*, and *htaA*. This strain also carries the pKN2.6Z plasmid harboring the WT full-length *hbpA* gene, specific point mutations of *hbpA*, or the empty vector (pKN). The four panels from *Top* to *Bottom* show the Coomassie stain, western blot with an anti-HbpA antibody, and in situ binding with Hb or with Hb–Hp followed by western blot with an anti-Hb or anti-Hp antibody, respectively. (*C*) Microscopy of wild-type *C. diphtheriae* strain 1737 (WT) (*Top*) and Δ*hbpA* (*Bottom*) *C. diphtheriae* cells. The figure shows images obtained using differential interference contrast (DIC) (*Left*), DAPI and α-Hb (Alexa Fluor 488) fluorescence (*Middle*), and a merge of the fluorescence images (*Right*). (*D*) Growth of *C. diphtheriae* Δ*hbpA* complemented with HbpA variant plasmids in iron-deplete media that contains the Hb–Hp complex as the sole iron source. For the determination of statistical significance, the growth levels of the mutants and the vector control were compared to the WT strain. Results show the mean and SD from at least three experiments, with statistical significance calculated using unpaired *t* tests; ***$P < 0.001$; **$P < 0.005$; ns, no significant difference. (*E*) Model of HbpA's interaction with Hb–Hp complex, constructed using the coordinates of our HbpA–Hb structure (PDB: 9BCJ) and the structure of the Hb–Hp complex (PDB: 4WJG) (51).

release from metHb is growth limiting, while hemin removal by HmuO and HrtAB presumably only affects the duration of the lag phase and the maximum achievable growth rate. Interestingly, when the metHb–Hp complex is provided as an iron source HbpA-dependent growth effects are observed (Fig. 6*D*). This is consistent with metHb–Hp complex releasing hemin more slowly than metHb, potentially increasing the growth benefits conferred by receptor-mediated tethering of this recalcitrant hemin source near the cell surface (57).

Discussion

To gain access to iron, pathogenic *C. diphtheriae* produces the HbpA receptor that binds to human Hb and the Hb–Hp complex (25). HbpA is required for optimal microbial growth when the Hb–Hp complex is provided as a sole source of iron and is unrelated to previously characterized Hb receptors based on its primary sequence. Here, we show using a combination of solution state NMR methods and X-ray crystallography that HbpA engages Hb

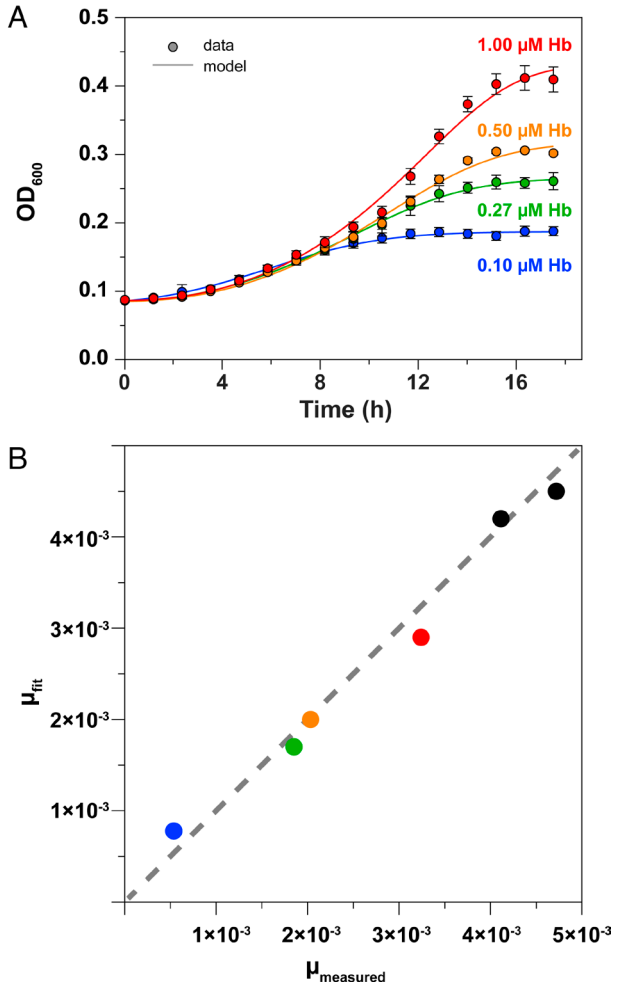

Fig. 7. *C. diphtheriae* scavenges hemin that is spontaneously released from Hb. (*A*) Growth experimental data vs. model predictions for *C. diphtheriae* grown on Hb. Experimental OD_{600} time points (circles) and model fit curves (solid lines) shown for Hb substrate concentrations of 0.10 μM (blue), 0.27 μM (green), 0.50 μM (orange), and 1.00 μM (red) (hemin units). Error bars show the SD obtained from three replicates. (*B*) Linear correlation plot of experimentally measured specific growth rates ($\mu_{measured}$) vs. the specific growth rates extracted from growth models assuming passive hemin release from Hb (μ_{fit}). The data and model are in good agreement (slope = 0.965, R^2 = 0.997). Modeling parameters are described in *SI Appendix*, Table S6, and sensitivity analysis of the parameters used to fit the growth data is presented in *SI Appendix*, Table S7.

via a structured N-terminal domain (residues 33 to 229, $HbpA^{\Delta 229}$). The molecular basis of binding is revealed by a 1.69 Å crystal structure of the 2:1 $HbpA^{\Delta 229}$–Hb complex in which each αHb subunit within the metHb tetramer is engaged by a single receptor. HbpA binding partially encapsulates the hemin bound to the αHb globins by contacting its D-ring propionate group, as well as surrounding globin residues located within and proximal to Hb's E- and F-helices. In situ binding studies reveal that the receptor–Hb contacts visualized in the crystal structure contribute to *C. diphtheriae*'s ability to capture Hb and the Hb–Hp complex, as four alanine substitutions in the receptor reduce cellular binding: Y52A, N55A, Y127A, and F206A (Fig. 6*A*). Based on NMR experiments, these contacts enable HbpA to interact with only the heme-bound form of Hb, while limiting binding to other types of heme-bound globins such as myoglobin (*SI Appendix*, Fig. S6). HbpA's preference for only the heme-loaded form of Hb may be advantageous, as it presumably enables *C. diphtheriae* to capture only iron-laden forms of Hb that can be used as a nutrient.

The results of in vitro hemin release measurements and Hb-dependent growth studies suggest that *C. diphtheriae* scavenges hemin after it is passively released from metHb. Consistent with the structure of the complex, biochemical experiments indicate that HbpA blocks hemin egress from the αHb subunit, while leaving spontaneous hemin loss from the βHb subunit unimpeded (Fig. 5 *C* and *D*). This specificity for αHb's hemin pocket presumably maximizes hemin flow into the cell, as only holo-metHb is tethered at the cell surface and hemin is spontaneously released from βHb ~10× faster than it is released from αHb (17). To determine whether cells harvest hemin through the passive process predicted by the biochemical and structural data, we mathematically modeled the dependence of bacterial growth on the rate of hemin release from metHb. This analysis revealed that *C. diphtheriae* growth is critically dependent on the kinetics of spontaneous hemin release from metHb—the microbe does not need to accelerate hemin release from metHb to explain the observed growth dependence (Fig. 7). Moreover, it explains why only modest growth defects are observed in 1737Δ*hbpA* cells when they are grown in batch cultures that contain Hb as an iron source. This is because in batch cultures released hemin rapidly diffuses to encounter cells for import, such that it does not matter if the hemin source (metHb) is bound to the cell surface by HbpA or free in the growth media as a result of genetically eliminating the receptor. At sites of infection the function of the receptor is presumably critical, since it enables the microbe to effectively compete with host proteins that bind and remove free metHb (Hp) and hemin (hemopexin, human serum albumin) (*SI Appendix*, Table S8) (18). Indeed, in contrast to Hb, modest and statistically significant defects in growth are observed when 1737Δ*hbpA* cells are cultured in media containing Hb–Hp as an iron source (Fig. 6). This observation is consistent with the fact that metHb–Hp releases hemin much more slowly than metHb (57), suggesting that tethering this recalcitrant hemin source near the microbe may facilitate growth by increasing the efficiency of hemin capture. In this scenario, so little hemin is released from metHb–Hp that optimizing hemin flow into the cell by tethering it to the surface via the receptor becomes advantageous, possibly by preventing hemin rebinding to the Hb–Hp complex or nonspecific hemin aggregation in the culture media. This is consistent with our finding that cells bearing Y127A and F206A receptor substitutions that disrupt Hb–Hp binding in situ also exhibit statistically significant reductions in their ability to use this iron source as a nutrient (Fig. 6). Notably, the importance of Y127 is consistent with recent studies of *C. diphtheriae* clinical isolates, as this position in their HbpA receptors exhibits a higher-level sequence conservation; the only documented variation at this position features a phenylalanine, conserving the aromatic nature of the side chain (50). In principle, the rate of hemin release from metHb and the Hb–Hp complex on the surface could also be facilitated by the unique environment present on the mycolic acid surface (58), and/or by the action of secreted or surface-displayed proteases that degrade Hb (59, 60).

Actinomycetota have evolved a parsimonious protein solution to capture metHb and hemin, since in *C. diphtheriae*'s hemin-uptake system our results reveal that these ligands are bound by structurally related HbpA and CR domains, respectively (Fig. 3). In the hemin-uptake system, five surface-displayed and secreted proteins scavenge hemin using CR domains (ChtA, ChtB, ChtC, HtaA, and HtaB). A comparison with HbpA reveals that both types of proteins adopt a similar β-sandwich fold and they employ related, but distinct distal subdomains to bind metHb and hemin (32, 33). Ligand binding appears to be very selective as hemin binding to HbpA is not observed when monitored by

UV-Vis spectroscopy (25), while NMR titration experiments show that a hemin-binding CR domain from the *C. diphtheriae* HtaA receptor does not interact with Hb (*SI Appendix*, Fig. S11) (61). These results indicate that either convergent or divergent evolution processes have shaped CR and HbpA proteins to adopt similar structural folds, each serving unique binding functions within the hemin uptake pathway. Interestingly, a similar evolutionary phenomenon has been observed in *Staphylococcus aureus*, as hemin uptake in this distantly related bacterium within the Bacillota phylum employs structurally divergent NEAT domains to bind to either metHb or hemin (61, 62).

Our results that support HbpA's localization on the cell surface are consistent with recent proteomics studies that define the positioning of protein components within *C. diphtheriae's* hemin uptake system (Fig. 6 *A* and *C*) (63). Those studies also place the ChtA, ChtC, and HtaA hemoproteins on the bacterial surface suggesting that they may scavenge hemin that is spontaneously released from metHb's β subunit when it is bound to HbpA, thus explaining why each of these proteins are essential for optimal bacterial growth when the metHb–Hp complex is provided as an iron source (Fig. 1) (24, 25, 40). Surface-scavenged hemin would then be relayed through the cell wall via HtaB or its paralog ChtB to the membrane-embedded HmuTUV complex for import into the cell and degradation. Interestingly, HbpA may have varied functions in hemin uptake, since a portion of the receptor is also secreted to form high molecular weight aggregates that avidly bind Hb (25, 52). These aggregates may be functionally important, since 1737Δ*hbpA* cell cultures that are supplied with exogenous full-length HbpA aggregates exhibit enhanced growth when Hb–Hp is provided as an iron source (52). Our results suggest that nonpolar interactions originating from residues within HbpA's C-terminal hydrophobic helix are required for extracellular aggregate formation (*SI Appendix*, Fig. S7). The nature of these aggregates remains unclear, but recent studies of the related bacterium *Corynebacterium glutamicum* have observed blebbing of protein-containing mycomembrane vesicles from its outer mycolic acid membrane that may function as nutrient delivery vectors (64). Thus, secreted HbpA receptors in *C. diphtheriae* may be embedded in mycomembrane vesicles that are capable of scavenging Hb from its surroundings, followed by return of the iron source via vesicle-microbial fusion.

The structure of HbpA differs from previously described Hb receptors (65–69). However, HbpA and other bacterial receptors appear to use a mechanistically similar strategy to maximize microbial recognition of hemin-loaded forms of metHb, while nevertheless enabling hemin capture from its βHb subunit. In particular, the Shr receptor from gram-positive *Streptococcus pyogenes* uses structurally unrelated Hemoglobin-interacting domain (HID) modules to selectively capture holo-metHb by contacting αHb, but like HbpA, when bound to Hb it does not block passive hemin loss from βHb (68). Similarly, the HpuA receptor in the gram-negative pathogen *Kingella dentrificans* may target βHb-bound hemin molecules for capture, since when bound to metHb the βHb-bound hemin molecules are left uncapped. Interestingly, βHb's labile hemin molecule has been proposed to be positioned near HpuB, an integral membrane protein that transports hemin through the outer membrane (69, 70). Thus, as highlighted in our studies of HbpA, this positioning may increase the efficiency of hemin flow into the cell and be particularly advantageous when the metHb–Hp complex is used as an iron source, and when competing host-encoded hemin-scavenging proteins are present (18). Alternative acquisition strategies are also employed by bacteria to scavenge Hb's hemin, as evidenced by the *S. aureus* IsdB and IsdH receptors which actively accelerate the rate of hemin release from metHb by distorting its hemin-binding pocket (49, 65, 66, 71–75). While it remains to be determined, it is conceivable that *S. aureus* requires higher rates of hemin consumption to grow effectively when colonizing its host, thereby making it advantageous for it to actively extract metHb's hemin. Future studies of the diverse mechanisms used by bacterial pathogens to acquire hemin from metHb promises to provide insight into how they colonize their human hosts, and could facilitate the development of urgently needed therapeutics to treat infections caused by multidrug-resistant bacteria.

Materials and Methods

Protein Preparations. Database identifiers for genes and proteins in this study are provided in *SI Appendix*, Table S4. Recombinant HbpA and HtaA proteins were expressed in *Escherichia coli* and purified using standard methods as described previously (33, 52). Human Hb was prepared from the blood of a healthy donor provided by the University of California Los Angeles/Centers for AIDS Research (UCLA/CFAR) Virology Core Laboratory, purified in the carbonmonoxy form (HbCO), and converted to metHb as previously described (49). H64Y/V68F myoglobin (apo-$Mb^{H64Y/V68F}$) was expressed and purified as previously described (49). Methyl ethyl ketone extraction was used to prepare apo-$Mb^{H64Y/V68F}$ and apo-Hb (76). Further details are described in *SI Appendix, Supplementary Materials and Methods*.

NMR Spectroscopy and Solution Structure Determination. NMR experiments were performed at 295 K on Bruker DRX 500 MHz, AVANCE III HD 600 MHz, and AVANCE NEO 800 MHz spectrometers each equipped with triple resonance cryogenic probes. Backbone chemical shift assignments of uniformly ^{15}N- and ^{13}C-labeled $HbpA^{\Delta 229}$ were determined from the following BEST-TROSY experiments: ^{1}H-^{15}N HSQC, HNCO, HN(CA)CO, HNCA, HN(CO)CA, HNCACB, HN(CO)CACB, and HBHA(CO)NH experiments (77–79). Sidechain assignments were made by acquiring and analyzing ^{15}N-TOCSY-HSQC, H(CCCO)NH, ^{1}H-^{13}C HSQC, HCCH-COSY, and HCCH-TOCSY spectra. 3D NOESY spectra acquired included 3D ^{15}N-edited, $^{13}C_{aliphatic}$-edited, and $^{13}C_{aromatic}$-edited experiments (100 ms mixing time for each). The solution structure was determined by automatic NOE assignment by ATNOS-CANDID algorithm in UNIO '10 (80–82), followed by manual NOE verification in XIPP and structure calculation in XPLOR-NIH (83–85). The final structure ensemble was deposited in the Protein Data Bank under PDB ID 9BCH. The DALI server was used to search for similar protein structures (86). Comparison to the AlphaFold Database model is presented in *SI Appendix*, Fig. S12. Further details are described in *SI Appendix, Supplementary Materials and Methods*.

Crystal Structure Determination of $HbpA^{\Delta 229}$–Hb Complex. $HbpA^{\Delta 229}$ complexed with HbCO was concentrated to 12 mg/mL for crystal screening in 20 mM HEPES, pH 8.0 buffer, and screened using the JCSG Plus screen (Molecular Dimensions), with hits further optimized. Final crystals were produced in 0.1 M Tris, pH 8.5, 0.24 M TMAO, 20% PEG-2000 MME, appearing after 2 to 3 d, and cryoprotected in reservoir solution containing 30% glycerol. Data were collected at the Advanced Photon Source on beamline 24-ID-C equipped with an EIGER2 X 16M detector at 100 K and processed using XDS and XSCALE to index, integrate, and scale reflections in the $P4_12_12$ space group (87). The dataset was anisotropic, so was further treated by ellipsoidal processing and anisotropic scaling using STARANISO (88). The structure was solved using molecular replacement with PHASER with the known structure of hemoglobin dimer (PDB: 2DN3) and refined using Coot and BUSTER (89–92). The coordinates and structure factors have been deposited in the Protein Data Bank under PDB ID 9BCJ. Complete statistics are presented in *SI Appendix*, Table S2. Additional details about crystallization, molecular replacement, and refinement are described in *SI Appendix, Supplementary Materials and Methods*.

Hemin Release and In Situ Hb Binding Measurements. The hemin release kinetics from Hb and the receptor–Hb complex were measured by monitoring changes to hemin's Soret band absorbance using an established plate reader assay as performed previously (68). Experiments were performed at 25 °C to avoid apo-globin aggregation. Hemin release from metHb occurs faster at 37 °C (k_{fast} ~ 15 vs. ~ 1 h^{-1}, k_{slow} ~ 0.6 vs. 0.1 h^{-1}). However, this does not change the results reported in this manuscript, as hemin release in the metHb–HbpA complex still occurs primarily from metHb's beta subunit at either 25 °C or 37 °C.

Hb and Hb–Hp binding to *C. diphtheriae* was determined by ELISA. Intact *C. diphtheriae* cells grown in low iron mPGT media were coated on a microtiter plate for an assessment of the surface exposure and binding capacity of HbpA proteins on the cell surface. As previously described (52), this method uses antibodies against HbpA for surface detection, while binding to Hb or Hb–Hp is assessed by incubation with each protein followed by detection by anti-Hb or anti-Hp antibodies, respectively. An alkaline phosphatase-labeled secondary antibody was used for detection, followed by the addition of pNPP and measurement of OD_{405}.

Gel Electrophoresis Assays of Cellular Fractions and Recombinant Proteins. Cells intended for analysis of supernatant and cellular fractions by in situ blotting were grown in low iron mPGT and normalized by OD_{600} at harvest. Cell pellets were lysed by treatment with lysozyme (from chicken egg white) and sodium lauroyl sarcosinate (Sarkosyl) as previously described (52). Lysed cells, supernatants, or purified proteins were run on precast PAGE TGX (Tris-glycine extended) gels (Bio–Rad) with a 4 to 15% gradient for separation under both denaturing and native conditions. These gels are manufactured without SDS and were run under native conditions by using native sample buffer (with no heating step) and Tris-glycine running buffer. Denaturing gels were run with samples boiled in Laemmli sample buffer for 10 min and separated using Tris-glycine running buffer (all reagents from Bio–Rad). Tween 20 (0.1%) was added to supernatant samples where indicated to allow protein aggregates to enter the gel. Coomassie blue staining, transfers to nitrocellulose, western blotting, and in situ analysis of Hb and Hb–Hp binding were performed as previously described (52).

***C. diphtheriae* Growth Studies.** The strains of *C. diphtheriae* and *Corynebacterium ulcerans* and relevant plasmids used in this study are listed in *SI Appendix*, Table S5. Complementation plasmids carrying *hbpA* point mutations and $HbpA^{\Delta 229}$ were constructed in the pKN2.6Z vector with the NEB HiFi DNA Assembly kit using one-fragment assembly cloning and the WT pKN-*hbpA* construct as source material for PCR (52). Primers were designed to introduce point mutations or delete the C-terminal sequence. Plasmids were transformed into *C. ulcerans* 712 to avoid HbpA toxicity to *E. coli*, verified by sequencing, then purified and electroporated into *C. diphtheriae* 1737. Strains were grown in heart infusion broth (Difco) with 0.2% Tween 80 (Millipore Sigma) (HIBTW) and stored with 20% glycerol at −80 °C. Iron-limited growth assays were done in a semidefined medium, mPGT, which has been previously described (93). Iron chloride ($FeCl_3$) was added at 0.25 μM for a low iron growth condition, and kanamycin was used at 50 μg/mL. Purified human Hb (MP Biomedical) was prepared to remove free hemin as described previously and used for growth at 4.37 μg/mL. Haptoglobin 1-1 (Athens Research and Technology) was used at 8.75 μg/mL (52). Terminal growth assays were conducted as previously described for *C. diphtheriae* 1737 (50). Details on Hb-dependent growth study in microtiter plate are described in *SI Appendix, Supplementary Materials and Methods*.

Data, Materials, and Software Availability. The NMR chemical shift assignments of $HbpA^{\Delta 229}$ have been deposited to the Biological Magnetic Resonance Data Bank (BMRB) under accession code 31164 (94). The solution NMR structure coordinates of apo $HbpA^{\Delta 229}$ have been deposited in the Protein Data Bank (PDB) under accession code 9BCH (95), while the coordinates and structure factors of the $HbpA^{\Delta 229}$–Hb complex crystal structure have been deposited with PDB code 9BCJ (96).

ACKNOWLEDGMENTS. We would like to thank members of the Clubb lab for useful discussions. This work was funded by grants from the NIH (R01AI161828 to R.T.C.) and in part by NIH National Institute of Dental & Craniofacial Research (NIDCR) (DE025015 to H.T.-T.). Additional support provided by NIH National Institute of General Medical Sciences (NIGMS)-funded predoctoral fellowships for J.F. (T32 GM145388), J.S. (T32 GM136614), N.A.C. (T32 GM145388 and T32 AI007323), and A.K.G. acknowledges support from the NIH NIDCR (T90DE030860). We also acknowledge NIH equipment grants S10OD025073 and S10OD016336 for partial support of the NMR core facilities. This research used resources at the University of California Los Angeles-United States Department of Energy (UCLA-DOE) Institute's X-ray and Electron Microscopy Structure Determination Core which is supported by the U.S. Department of Energy (DE-FC02-02ER63421). The X-ray diffraction experiments were performed at the NIH NIGMS-funded Northeastern Collaborative Access Team beamlines (P30 GM124165). The research used resources of the Advanced Photon Source, a U.S. DOE Office of Science User Facility operated for the DOE Office of Science by Argonne National Laboratory under Contract number DE-AC02-06CH11357.

1. W. J. Class, Clinical significance of the different forms of the Klebs-Loeffler bacillus. *J. Am. Med. Associat.*, 1019–1020 (1898).
2. M. P. Schmitt, "Iron acquisition and iron-dependent gene expression in Corynebacterium diphtheriae" in *Corynebacterium Diphtheriae and Related Toxigenic Species: Genomics, Pathogenicity and Applications*, A. Burkovski, Ed. (Springer Netherlands, 2014), pp. 95–121.
3. L. Barksdale, Corynebacterium diphtheriae and its relatives. *Bacteriol. Rev.* **34**, 378–422 (1970).
4. C. A. Kunkle, M. P. Schmitt, Analysis of the Corynebacterium diphtheriae DtxR regulon: Identification of a putative siderophore synthesis and transport system that is similar to the yersinia high-pathogenicity island-encoded Yersiniabactin synthesis and uptake system. *J. Bacteriol.* **185**, 6826–6840 (2003).
5. C. A. Kunkle, M. P. Schmitt, Analysis of a DtxR-regulated iron transport and siderophore biosynthesis gene cluster in Corynebacterium diphtheriae. *J. Bacteriol.* **187**, 422–433 (2005).
6. J. Boyd, M. N. Oza, J. R. Murphy, Molecular cloning and DNA sequence analysis of a diphtheria tox iron-dependent regulatory element (dtxR) from Corynebacterium diphtheriae. *Proc. Natl. Acad. Sci. U.S.A.* **87**, 5968–5972 (1990).
7. M. P. Schmitt, R. K. Holmes, Iron-dependent regulation of diphtheria toxin and siderophore expression by the cloned Corynebacterium diphtheriae repressor gene dtxR in C. diphtheriae C7 strains. *Infect. Immun.* **59**, 1899–1904 (1991).
8. N. L. Parrow, R. E. Fleming, M. F. Minnick, Sequestration and scavenging of iron in infection. *Infect. Immun.* **81**, 3503–3514 (2013).
9. H. Contreras, N. Chim, A. Credali, C. W. Goulding, Heme uptake in bacterial pathogens. *Curr. Opin. Chem. Biol.* **19**, 34–41 (2014).
10. C. Wandersman, P. Delepelaire, "Heme-delivering proteins in bacteria" in *Handbook of Porphyrin Science*, G. C. Ferreira, Ed. (World Scientific Publishing Company, 2012), pp. 191–222.
11. L. Ma, A. Terwilliger, A. W. Maresso, Iron and zinc exploitation during bacterial pathogenesis. *Metallomics* **7**, 1541–1554 (2015).
12. J. R. Sheldon, D. E. Heinrichs, Recent developments in understanding the iron acquisition strategies of gram positive pathogens. *FEMS Microbiol. Rev.* **39**, 592–630 (2015).
13. J. E. Choby, E. P. Skaar, Heme synthesis and acquisition in bacterial pathogens. *J. Mol. Biol.* **428**, 3408–3428 (2016).
14. J. R. Sheldon, H. A. Laakso, D. E. Heinrichs, "Iron acquisition strategies of bacterial pathogens" in *Virulence Mechanisms of Bacterial Pathogens*, I. T. Kudva *et al.*, Eds. (John Wiley & Sons Ltd, 2016), pp. 43–85.
15. W. Huang, A. Wilks, Extracellular heme uptake and the challenge of bacterial cell membranes. *Annu. Rev. Biochem.* **86**, 799–823 (2017).
16. P. Hensley, S. J. Edelstein, D. C. Wharton, Q. H. Gibson, Conformation and spin state in methemoglobin. *J. Biol. Chem.* **250**, 952–960 (1975).
17. M. S. Hargrove, T. Whitaker, J. S. Olson, R. J. Vali, A. J. Mathews, Quaternary structure regulates hemin dissociation from human hemoglobin. *J. Biol. Chem.* **272**, 17385–17389 (1997).
18. I. S. Pires, F. Berthiaume, A. F. Palmer, Engineering therapeutics to detoxify hemoglobin, heme, and iron. *Annu. Rev. Biomed. Eng.* **25**, 1–21 (2023).
19. P. W. Buehler, E. Karnaukhova, When might transferrin, hemopexin or haptoglobin administration be of benefit following the transfusion of red blood cells? *Curr. Opin. Hematol.* **25**, 452 (2018).
20. M. Kristiansen *et al.*, Identification of the haemoglobin scavenger receptor. *Nature* **409**, 198–201 (2001).
21. C. B. F. Andersen *et al.*, Structure of the haptoglobin–haemoglobin complex. *Nature* **489**, 456–459 (2012).
22. D. J. Schaer, P. W. Buehler, A. I. Alayash, J. D. Belcher, G. M. Vercellotti, Hemolysis and free hemoglobin revisited: Exploring hemoglobin and hemin scavengers as a novel class of therapeutic proteins. *Blood* **121**, 1276–1284 (2013).
23. K. L. Sædrup *et al.*, The Staphylococcus aureus protein IsdH inhibits host hemoglobin scavenging to promote heme acquisition by the pathogen. *J. Biol. Chem.* **291**, 23989–23998 (2016).
24. C. E. Allen, M. P. Schmitt, Utilization of host iron sources by Corynebacterium diphtheriae: Multiple hemoglobin-binding proteins are essential for the use of iron from the hemoglobin-haptoglobin complex. *J. Bacteriol.* **197**, 553–562 (2015).
25. L. R. Lyman, E. D. Peng, M. P. Schmitt, Corynebacterium diphtheriae iron-regulated surface protein HbpA is involved in the utilization of the hemoglobin-haptoglobin complex as an iron source. *J. Bacteriol.* **200**, e00676-17 (2018).
26. D. Akinbosede, R. Chizea, S. A. Hare, Pirates of the haemoglobin. *Microb. Cell* **9**, 84–102 (2022).
27. M. A. Andrade, F. D. Ciccarelli, C. Perez-Iratxeta, P. Bork, NEAT: A domain duplicated in genes near the components of a putative Fe3+siderophore transporter from Gram-positive pathogenic bacteria *Genome Biol.* **3**, research0047.1 (2002).
28. K. Ellis-Guardiola, B. J. Mahoney, R. T. Clubb, NEAr transporter (NEAT) domains: Unique surface displayed heme chaperones that enable gram-positive bacteria to capture heme-iron from hemoglobin. *Front. Microbiol.* **11**, 607679 (2021).
29. E. S. Drazek, C. A. Hammack Sr., M. P. Schmitt, Corynebacterium diphtheriae genes required for acquisition of iron from haemin and haemoglobin are homologous to ABC haemin transporters. *Mol. Microbiol.* **36**, 68–84 (2000).
30. M. P. Schmitt, E. S. Drazek, Construction and consequences of directed mutations affecting the hemin receptor in pathogenic corynebacterium species. *J. Bacteriol.* **183**, 1476–1481 (2001).
31. C. E. Allen, M. P. Schmitt, HtaA is an iron-regulated hemin binding protein involved in the utilization of heme iron in Corynebacterium diphtheriae. *J. Bacteriol.* **191**, 2638–2648 (2009).
32. N. Muraki *et al.*, Structural basis for the heme transfer reaction in heme uptake machinery from Corynebacteria. *Chem. Commun.* **55**, 13864–13867 (2019).
33. B. J. Mahoney *et al.*, Development and atomic structure of a new fluorescence-based sensor to probe heme transfer in bacterial pathogens. *J. Inorg. Biochem.* **249**, 112368 (2023).
34. C. E. Allen, M. P. Schmitt, Novel hemin binding domains in the Corynebacterium diphtheriae HtaA Protein interact with hemoglobin and are critical for heme iron utilization by HtaA. *J. Bacteriol.* **193**, 5374–5385 (2011).
35. R. C. Uluisik *et al.*, Characterization of the second conserved domain in the heme uptake protein HtaA from Corynebacterium diphtheriae. *J. Inorg. Biochem.* **167**, 124–133 (2017).

36. C. A. Kunkle, M. P. Schmitt, Comparative analysis of hmuO function and expression in Corynebacterium species. *J. Bacteriol.* **189**, 3650–3654 (2007).
37. A. Wilks, M. P. Schmitt, Expression and characterization of a heme oxygenase (Hmu O) from Corynebacterium diphtheriae: Iron acquisition requires oxidative cleavage of the heme macrocycle. *J. Biol. Chem.* **273**, 837–841 (1998).
38. M. P. Schmitt, Utilization of host iron sources by Corynebacterium diphtheriae: Identification of a gene whose product is homologous to eukaryotic heme oxygenases and is required for acquisition of iron from heme and hemoglobin. *J. Bacteriol.* **179**, 838–845 (1997).
39. S. Dittmann *et al.*, Successful control of epidemic diphtheria in the states of the Former Union of Soviet Socialist Republics: Lessons learned. *J. Infect. Dis.* **181**, S10–S22 (2000).
40. C. E. Allen, J. M. Burgos, M. P. Schmitt, Analysis of novel iron-regulated, surface-anchored hemin-binding proteins in Corynebacterium diphtheriae. *J. Bacteriol.* **195**, 2852–2863 (2013).
41. L. A. Bibb, M. P. Schmitt, The ABC transporter HrtAB confers resistance to hemin toxicity and is regulated in a hemin-dependent manner by the ChrAS two-component system in Corynebacterium diphtheriae. *J. Bacteriol.* **192**, 4606–4617 (2010).
42. J. M. Burgos, M. P. Schmitt, The ChrA response regulator in Corynebacterium diphtheriae controls hemin-regulated gene expression through binding to the hmuO and hrtAB promoter regions. *J. Bacteriol.* **194**, 1717–1729 (2012).
43. E. Krissinel, K. Henrick, Inference of macromolecular assemblies from crystalline state. *J. Mol. Biol.* **372**, 774–797 (2007).
44. E. Krissinel, Crystal contacts as nature's docking solutions. *J. Comput. Chem.* **31**, 133–143 (2010).
45. N. Shibayama, A. Sato-Tomita, M. Ohki, K. Ichiyanagi, S.-Y. Park, Direct observation of ligand migration within human hemoglobin at work. *Proc. Natl. Acad. Sci. U.S.A.* **117**, 4741–4748 (2020).
46. M. A. Herzik, M. Wu, G. C. Lander, High-resolution structure determination of sub-100 kDa complexes using conventional cryo-EM. *Nat. Commun.* **10**, 1032 (2019).
47. P. P. Samuel *et al.*, The interplay between molten globules and heme disassociation defines human hemoglobin disassembly. *Biophys. J.* **118**, 1381–1400 (2020).
48. M. S. Hargrove *et al.*, His 64(E7)–>Tyr apomyoglobin as a reagent for measuring rates of hemin dissociation. *J. Biol. Chem.* **269**, 4207–4214 (1994).
49. M. Sjodt *et al.*, Energetics underlying hemin extraction from human hemoglobin by Staphylococcus aureus. *J. Biol. Chem.* **293**, 6942–6957 (2018).
50. L. R. Lyman, J. Schaeffer, W. Ruppitsch, M. P. Schmitt, Analysis of the HbpA protein from Corynebacterium diphtheriae clinical isolates and identification of a putative hemoglobin-binding site on HbpA. *J. Bacteriol.* **204**, e00349-22 (2022).
51. K. Stødkilde, M. Torvund-Jensen, S. K. Moestrup, C. B. F. Andersen, Structural basis for trypanosomal haem acquisition and susceptibility to the host innate immune system. *Nat. Commun.* **5**, 5487 (2014).
52. L. R. Lyman, E. D. Peng, M. P. Schmitt, The Corynebacterium diphtheriae HbpA hemoglobin-binding protein contains a domain that is critical for hemoprotein binding, cellular localization, and function. *J. Bacteriol.* **203**, e0019621 (2021), 10.1128/jb.00196-21.
53. J. C. Mocny, J. S. Olson, T. D. Connell, Passively released heme from hemoglobin and myoglobin is a potential source of nutrient iron for Bordetella bronchiseptica. *Infect. Immun.* **75**, 4857–4866 (2007).
54. J. Monod, The growth of bacterial cultures. *Annu. Rev. Microbiol.* **3**, 371–394 (1949).
55. Y. Liu, Overview of some theoretical approaches for derivation of the Monod equation. *Appl. Microbiol. Biotechnol.* **73**, 1241–1250 (2007).
56. M. Keppel, H. Piepenbreier, C. Gätgens, G. Fritz, J. Frunzke, Toxic but tasty–Temporal dynamics and network architecture of heme-responsive two-component signaling in Corynebacterium glutamicum. *Mol. Microbiol.* **111**, 1367–1381 (2019).
57. T. L. Mollan *et al.*, Redox properties of human hemoglobin in complex with fractionated dimeric and polymeric human haptoglobin. *Free Radical Biol. Med.* **69**, 265–277 (2014).
58. K. C. Rahlwes, I. L. Sparks, Y. S. Morita, "Cell walls and membranes of actinobacteria" in *Bacterial Cell Walls and Membranes*, A. Kuhn, Ed. (Springer International Publishing, Subcellular Biochemistry, 2019), vol. 92, pp. 417–469.
59. T. Olczak, D. W. Dixon, C. A. Genco, Binding specificity of the Porphyromonas gingivalis heme and hemoglobin receptor HmuR, gingipain K, and gingipain R1 for heme, porphyrins, and metalloporphyrins. *J. Bacteriol.* **183**, 5599–5608 (2001).
60. M. Paramaesvaran *et al.*, Porphyrin-mediated cell surface heme capture from hemoglobin by Porphyromonas gingivalis. *J. Bacteriol.* **185**, 2528–2537 (2003).
61. R. Macdonald, B. J. Mahoney, K. Ellis-Guardiola, A. Maresso, R. T. Clubb, NMR experiments redefine the hemoglobin binding properties of bacterial NEAr-iron transporter domains. *Protein Sci.* **28**, 1513–1523 (2019).
62. E. S. Honsa, A. W. Maresso, S. K. Highlander, Molecular and evolutionary analysis of NEAr-iron transporter (NEAT) domains. *PLoS One* **9**, e104794 (2014).
63. A. K. Goring *et al.*, The exoproteome and surfaceome of toxigenic corynebacterium diphtheriae 1737 and its response to iron restriction and growth on human hemoglobin. *J. Proteome Res.* (2024). https://doi.org/10.1021/acs.jproteome.4c00443.
64. K. Kawashima, T. Nagakubo, N. Nomura, M. Toyofuku, Iron delivery through membrane vesicles in Corynebacterium glutamicum. *Microbiol. Spectrum* **11**, e01222-23 (2023).
65. C. F. Dickson, D. A. Jacques, R. T. Clubb, J. M. Guss, D. A. Gell, The structure of haemoglobin bound to the haemoglobin receptor IsdH from Staphylococcus aureus shows disruption of the native α-globin haem pocket. *Acta Cryst. D* **71**, 1295–1306 (2015).
66. C. F. M. Bowden *et al.*, Structure–function analyses reveal key features in Staphylococcus aureus IsdB-associated unfolding of the heme-binding pocket of human hemoglobin. *J. Biol. Chem.* **293**, 177–190 (2018).
67. O. De Bei *et al.*, Cryo-EM structures of staphylococcal IsdB bound to human hemoglobin reveal the process of heme extraction. *Proc. Natl. Acad. Sci. U.S.A.* **119**, e2116708119 (2022).
68. R. Macdonald *et al.*, The Shr receptor from Streptococcus pyogenes uses a cap and release mechanism to acquire heme–iron from human hemoglobin. *Proc. Natl. Acad. Sci. U.S.A.* **120**, e2211939120 (2023).
69. C. T. Wong *et al.*, Structural analysis of haemoglobin binding by HpuA from the Neisseriaceae family. *Nat. Commun.* **6**, 10172 (2015).
70. L. A. Lewis, E. Gray, Y.-P. Wang, B. A. Roe, D. W. Dyer, Molecular characterization of hpuAB, the haemoglobin–haptoglobin-utilization operon of Neisseria meningitidis. *Mol. Microbiol.* **23**, 737–749 (1997).
71. C. F. Dickson *et al.*, Structure of the hemoglobin-IsdH complex reveals the molecular basis of iron capture by Staphylococcus aureus. *J. Biol. Chem.* **289**, 6728–6738 (2014).
72. K. Ellis-Guardiola *et al.*, The *Staphylococcus aureus* IsdH receptor forms a dynamic complex with human hemoglobin that triggers heme release via two distinct hot spots. *J. Mol. Biol.* **432**, 1064–1082 (2020).
73. J. Clayton *et al.*, Directed inter-domain motions enable the IsdH *Staphylococcus aureus* receptor to rapidly extract heme from human hemoglobin. *J. Mol. Biol.* **434**, 167623 (2022).
74. T. Spirig *et al.*, *Staphylococcus aureus* uses a novel multidomain receptor to break apart human hemoglobin and steal its heme. *J. Biol. Chem.* **288**, 1065–1078 (2013).
75. E. Gianquinto *et al.*, Interaction of human hemoglobin and semi-hemoglobins with the Staphylococcus aureus hemophore IsdB: A kinetic and mechanistic insight. *Sci. Rep.* **9**, 18629 (2019).
76. F. W. J. Teale, Cleavage of the haem-protein link by acid methylethylketone. *Biochim. Biophys. Acta* **35**, 543 (1959).
77. P. Schanda, H. Van Melckebeke, B. Brutscher, Speeding up three-dimensional protein NMR experiments to a few minutes. *J. Am. Chem. Soc.* **128**, 9042–9043 (2006).
78. P. Schanda, Fast-pulsing longitudinal relaxation optimized techniques: Enriching the toolbox of fast biomolecular NMR spectroscopy. *Prog. Nucl. Magn. Reson. Spectrosc.* **55**, 238–265 (2009).
79. J. Cavanagh, *Protein NMR Spectroscopy: Principles and Practice* (Academic Press, 1996).
80. P. Guerry, T. Herrmann, "Comprehensive automation for NMR structure determination of proteins" in *Protein NMR Techniques*, A. Shekhtman, D. S. Burz, Eds. (Humana Press, *Methods in Molecular Biology*, 2012), vol. 831, pp. 429–451.
81. T. Herrmann, P. Güntert, K. Wüthrich, Protein NMR structure determination with automated NOE-identification in the NOESY spectra using the new software ATNOS. *J. Biomol. NMR* **24**, 171–189 (2002).
82. T. Herrmann, P. Güntert, K. Wüthrich, Protein NMR structure determination with automated NOE assignment using the new software CANDID and the torsion angle dynamics algorithm DYANA. *J. Mol. Biol.* **319**, 209–227 (2002).
83. C. D. Schwieters, J. J. Kuszewski, N. Tjandra, G. Marius Clore, The Xplor-NIH NMR molecular structure determination package. *J. Magn. Reson.* **160**, 65–73 (2003).
84. C. D. Schwieters, J. J. Kuszewski, G. Marius Clore, Using Xplor–NIH for NMR molecular structure determination. *Prog. Nucl. Magn. Reson. Spectrosc.* **48**, 47–62 (2006).
85. D. S. Garrett, M. Cai, G. M. Clore, XIPP: Multi-dimensional NMR analysis software. *J. Biomol. NMR* **74**, 9–25 (2020).
86. L. Holm, Dali server: Structural unification of protein families. *Nucleic Acids Res.* **50**, W210–W215 (2022).
87. W. Kabsch, XDS. *Acta Cryst. D* **66**, 125–132 (2010).
88. I. J. Tickle *et al.*, STARANISO (Version 3.350, Global Phasing Ltd., Cambridge, UK, 2023).
89. P. Emsley, B. Lohkamp, W. G. Scott, K. Cowtan, Features and development of Coot. *Acta Cryst. D* **66**, 486–501 (2010).
90. G. Bricogne *et al.*, BUSTER (Version 2.10.4, Global Phasing Ltd., Cambridge, UK, 2023).
91. A. J. McCoy *et al.*, Phaser crystallographic software. *J. Appl. Cryst.* **40**, 658–674 (2007).
92. S.-Y. Park, T. Yokoyama, N. Shibayama, Y. Shiro, J. R. H. Tame, 1.25 Å resolution crystal structures of human haemoglobin in the oxy, deoxy and carbonmonoxy forms. *J. Mol. Biol.* **360**, 690–701 (2006).
93. S.-P.S. Tai, A. E. Krafft, P. Nootheti, R. K. Holmes, Coordinate regulation of siderophore and diphtheria toxin production by iron in *Corynebacterium diphtheriae*. *Microb. Pathog.* **9**, 267–273 (1990).
94. B. J. Mahoney, R. T. Clubb, Solution structure of the hemoglobin receptor HbpA from Corynebacterium diphtheria. Biological Magnetic Resonance Data Bank (BMRB). https://doi.org/10.13018/BMR31164. Deposited 9 April 2024.
95. B. J. Mahoney, R. T. Clubb, Solution structure of the hemoglobin receptor HbpA from Corynebacterium diphtheriae. Worldwide Protein Data Bank (wwPDB). https://doi.org/10.2210/pdb9bch/pdb. Deposited 9 April 2024.
96. B. J. Mahoney, D. Cascio, R. T. Clubb, Crystal structure of human hemoglobin in complex with the HbpA receptor from Corynebacterium diphtheriae. Worldwide Protein Data Bank (wwPDB). https://doi.org/10.2210/pdb9bcj/pdb. Deposited 9 April 2024.